Supplementary material

Influence of synthesis method on the structural characteristics of novel hybrid adsorbents based on bentonite

Dariusz Sternik[1], Mariia Galaburda[2]*, Viktor M. Bogatyrov[2], Volodymyr M. Gun'ko[2]

[1] Faculty of Chemistry, Maria Curie-Skłodowska University, Maria Curie-Sklodowska Sq.3, 20-031 Lublin, Poland; dsternik@poczta.umcs.lublin.pl

[2] Chuiko Institute of Surface Chemistry, NAS of Ukraine, 17 General Naumov Str., Kyiv 03164, Ukraine; mariia.galaburda@gmail.com

* Correspondence: mariia.galaburda@gmail.com; Tel.: +30444229672.

Table S1. The ratio of the initial components used to prepare composites.

Name	Bentonite (g)	Resorcinol (g)	Formaldehyde (g)	Water (g)	The yield of RFC after pyrolysis (%)	Polymer content (%)
RFR-75	10.02	10.04	15.00	–	55.55	52.44
RFR-76	10.00	6.00	9.02	6.05	54.15	40.08
RFR-77	10.00	3.00	4.53	11.32	50.82	28.01
RFR-78	10.00	10.03	15.03	–	66.50	55.74
RFR-79	10.00	6.00	15.01	–	67.88	46.3
RFR-80	10.00	3.01	15.26	–	71.26	32.36
Polymer	–	10.00	15.01	10.01	50.86	

Small-angle X-ray scattering (SAXS)

The differential pore size distribution (PSD) functions $f(r)$ based on the small-angle X-ray scattering (SAXS) data (Fig. S1) were calculated (Fig. S2) using Fredholm integral equation of the first kind for scattering intensity $I(q)$ [1]

$$I(q) = C\int_{r_{min}}^{r_{max}} \frac{\left(\sin qr - qr\cos qr\right)^2}{(qr)^2} V(r) f(r) dr, \qquad \text{(S1)}$$

where C is a constant, $q = 4\pi\sin(\theta)/\lambda$ the scattering vector value, 2θ is the scattering angle λ is the wavelength of incident X-ray, $V(r)$ is the volume of a pore with radius r (proportional to r^3), and $f(r)dr$ represents the probability of having pores with radius r to $r + dr$. The values of r_{min} (= π/q_{max}) and r_{max} (= π/q_{min}) correspond to lower and upper limits of the resolvable real space due to instrument resolution. This equation was solved using the CONTIN algorithm [2]. The $f(r)$ function could be converted into incremental PSD (IPSD) $\Phi(r_i) = (f(r_{i+1}) + f_V(r_i))(r_{i+1} - r_i)/2$ for better view of the PSD at larger r values.

The chord size distribution, $G(r)$ as a geometrical statistic description of a multiphase medium, was calculated from the SAXS data [3,4]

$$G(r) = C\int_0^{\infty}\left[K - q^4 I(q)\right]\frac{d^2}{dr^2}\left(-4\frac{\sin qr}{qr}\right)dq, \qquad \text{(S2)}$$

where K is the Porod constant (corresponding to scattering intensity $I(q) \sim Kq^{-4}$ in the Porod range).

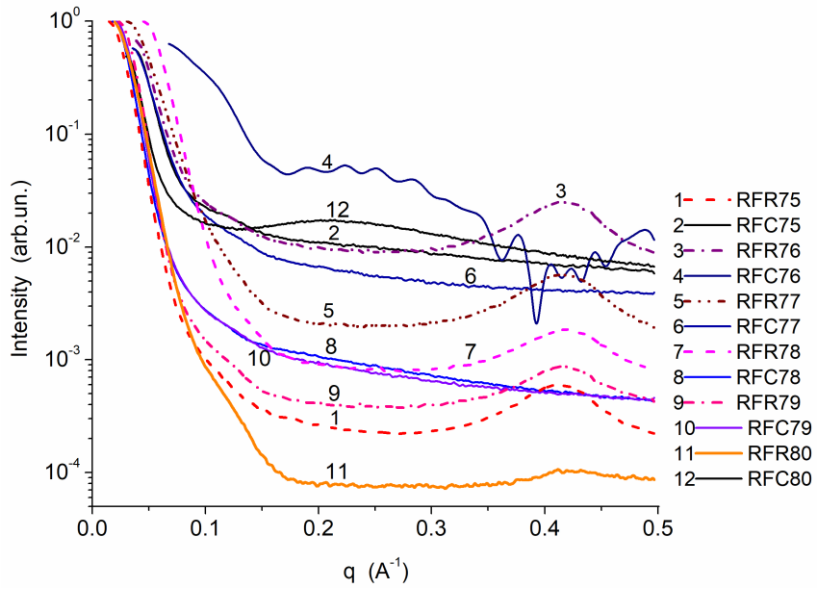

Figure S1. Normalized SAXS curves for initial RFR and related carbonized samples RFC.

The specific surface area from the SAXS data was calculated (in m^2/g) using equation

$$S_{SAXS} = 10^4 \pi\phi(1-\phi)\frac{K}{Q\rho_a}, \qquad \text{(S3)}$$

where $\phi = \rho_\alpha/\rho_0$ is the solid fraction of adsorbent, and Q is the invariant

$$Q = \int_0^{\infty} q^2 I(q)dq\,. \qquad \text{(S4)}$$

The Q value is sensitive to the range used on integration of Eq. (S4) (since experimental q values are measured between the q_{min} and q_{max} values different from 0 and ∞). Therefore, the invariant value Q was calculated using equation [5]

$$Q = \sum_{q_{min}}^{q_{max}} (I(q_i) - b)q_i^2 \Delta q_i + K / q_{max} \qquad \text{(S5)}$$

where b is a constant determined using equation

$$I(q)q^4 = K + bq^4 \qquad \text{(S6)}$$

valid in the Porod range.

To calculate the particle size distribution (PaSD) functions (Fig. S3), several models of particles (e.g. spherical, cylindrical, lamellar ones and various blends of them) could be used. For spherical particles, integral equation similar to eq. (S1) could be written as follows

$$I(q) = C \int_{R_{\min}}^{R_{\max}} P(q,R) f(R) dR , \qquad \text{(S7)}$$

where C is a constant, R is the radius of particles, $f(R)$ is the distribution function (differential PaSD), and $P(R)$ is the form factor for spherical particles [6] (the kernel of the integral equation S7): $P(q,R) = (4\pi R^3/3)^2[\Phi(q)]^2$ and $\Phi(q,R) = (3/(qR)^3)[\sin(qR) - qR\cos(qR)]$.

The PaSD with respect to the volume of particles (as abundance in vol%) could be calculated as follows abundance

$$\text{(vol\%)} = R^3 f(R) / \int R^3 f(R) dR . \qquad \text{(S8)}$$

For cylindrical particles, there are two variable parameters, such as the radius (R) and length (H) of cylinders

$$I(q) = C \int_{H_{\min}}^{H_{\max}} \int_{R_{\min}}^{R_{\max}} f(H) f(R) P(q,H,R) dH dR , \qquad \text{(S9)}$$

$$P(q,H,R) = CV \int_0^{\pi/2} \frac{2J_1(qR\sin\theta)}{qR\sin\theta} \frac{\sin\left(0.5qH\cos\theta\right)}{0.5qH\cos\theta} \sin\theta d\theta$$

where, $J_1(x)$ is the first-order Bessel function, $V = \pi R^2 H$ is the cylinder volume, and C is a constant [6].

For lamellar particles [6]

$$I(q) = C \int_{L_{\min}}^{L_{\max}} P(q,L) f(L) dL , \qquad \text{(S10)}$$

where $P(q,L) = (L/q)^2 \left[\frac{\sin(qL/2)}{(qL/2)} \right]^2$, L is the lamellar thickness, and the prefactor ($1/q^2$) is the so-called Lorentz factor required to randomize the orientation of the lamellar particle [6]. In the case of complex systems, several models with various blends of spherical, cylindrical and lamellar particles could be used with certain weight coefficients (Table S2), which were determined using self-consistent regularization procedure described elsewhere [7].

Note that the SAXS treatments described above were successfully used for carbon, silica, and polymeric materials in comparison with the results of various methods used to analyze the nitrogen adsorption and ^{1}H NMR cryoporometry data [8-11].

Table S2. Weight coefficients in the PaSD (model with lamellar(lam), cylindrical (cyl) and spherical (sph) particles) calculated using the self-consistent regularization procedure

Sample	c_{lam}	c_{cyl}	c_{sph}
RFR-75	0.036	0.085	0.879
RFR-76	0.225	0.383	0.392
RFR-77	0.481	0.170	0.349
RFR-78	0.475	0.317	0.208
RFR-79	0.188	0.308	0.505
RFR-80	0.001	0.061	0.938
RFC-75	0.654	0.133	0.213
RFC-76	0.907	0.007	0.086
RFC-77	0.468	0.224	0.308
RFC-78	0.088	0.118	0.794
RFC-79	0.171	0.262	0.567
RFC-80	0.588	0.199	0.213

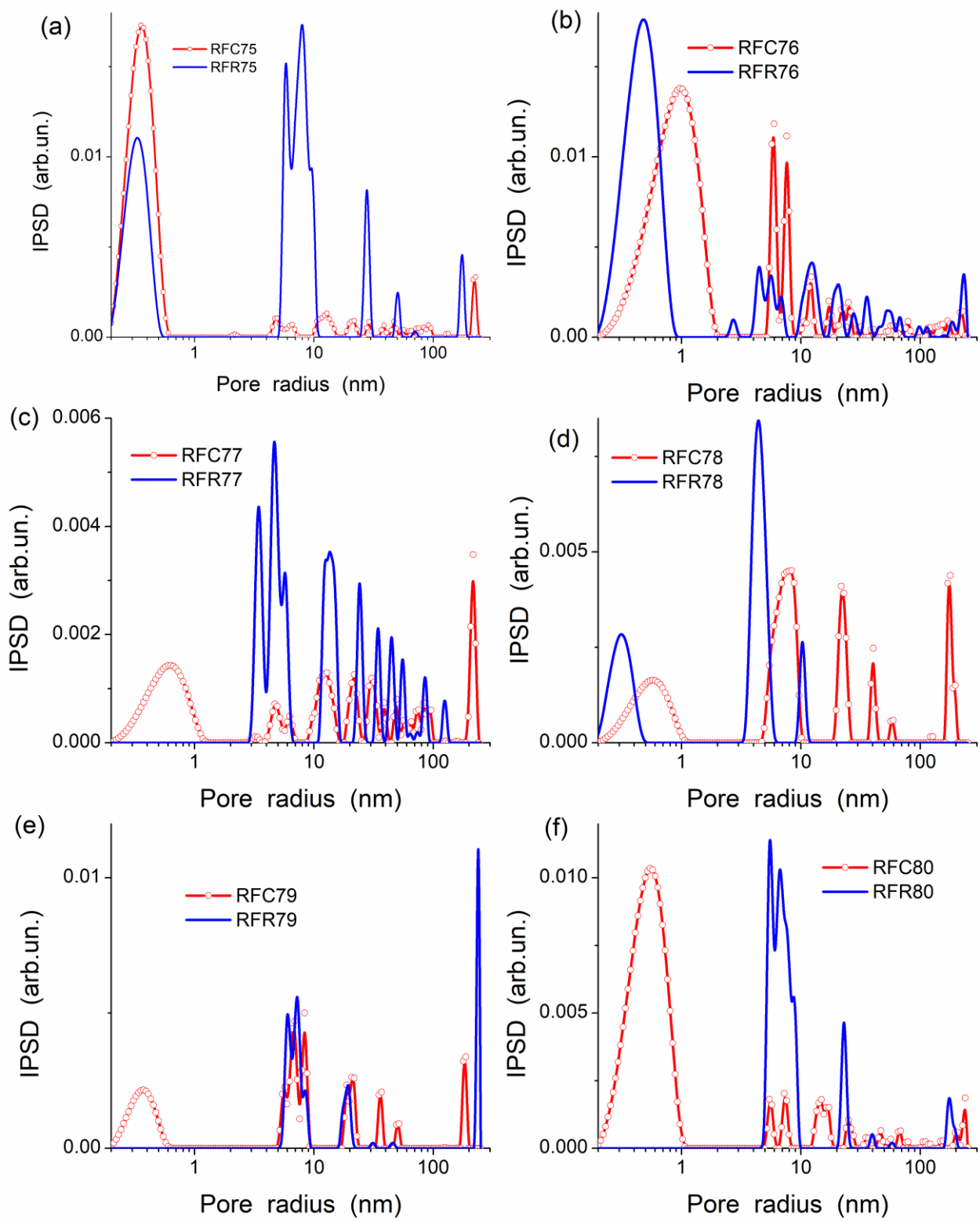

Figure S2. Incremental pore size distributions calculated using the SAXS data.

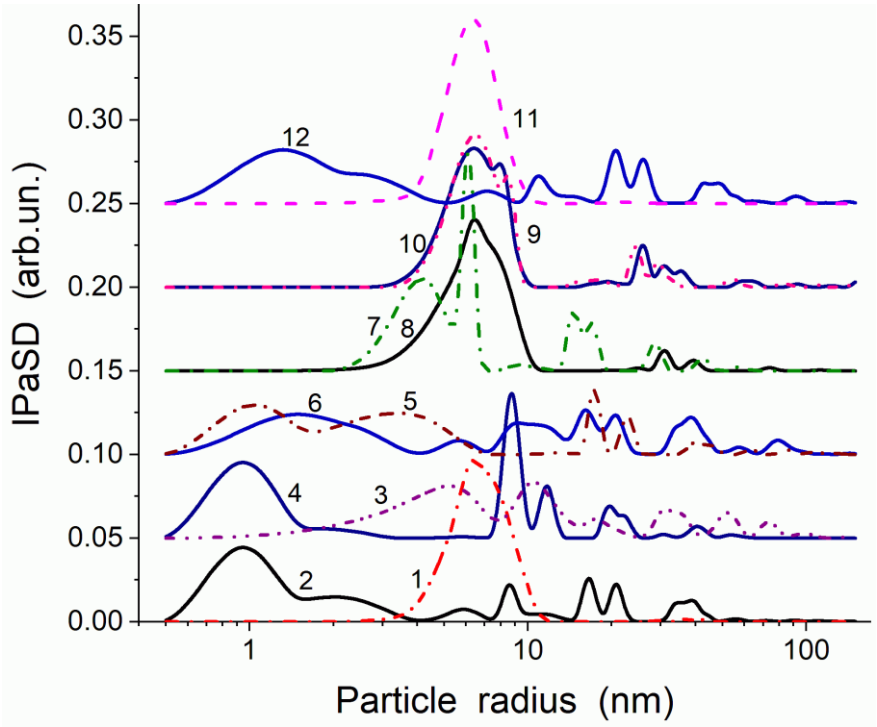

Figure S3. Particle size distributions (with a complex model of lamellar, spherical and cylindrical nanoparticles) calculated using the SAXS data: curves 1 – RFR75, 2 - RFRC75, 3 – RFR76, 4 – RFC76, 5 -RFR77, 6 – RFC76, 7 – RFR77, 8 – RFC78, 9 – RFR79, 10 – RFC79, 11 – RFR80, 12 – RFC80.

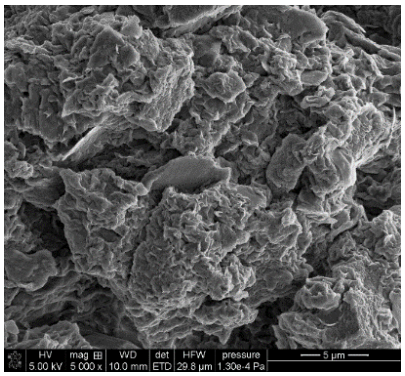

RFR-75

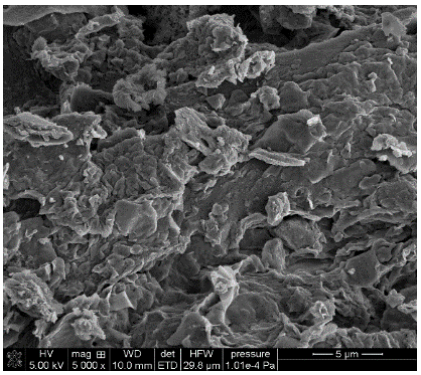

RFC-75

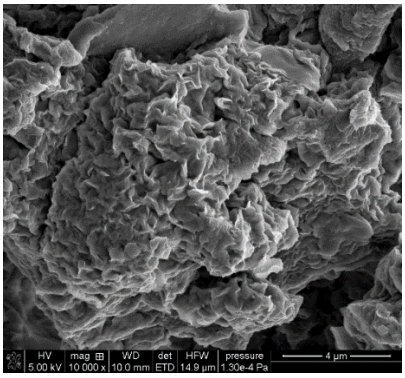

RFR-76

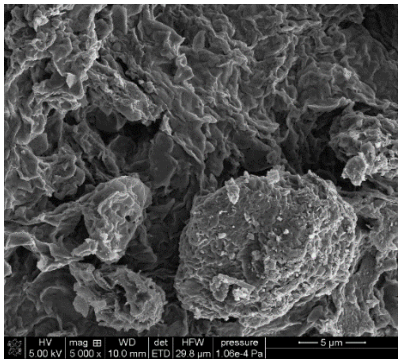

RFC-76

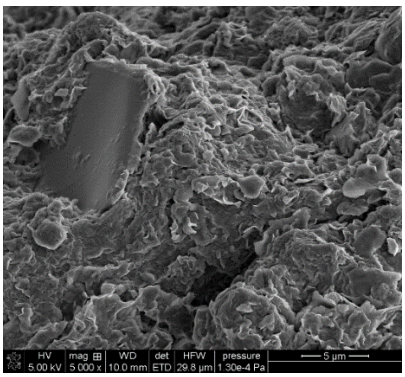
RFR-77

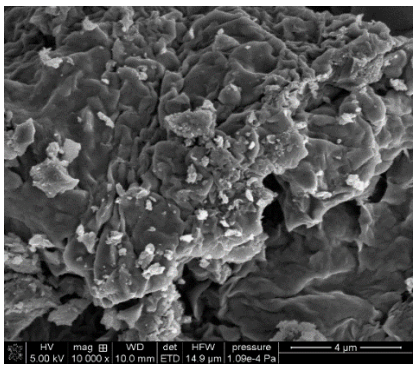
RFC-77

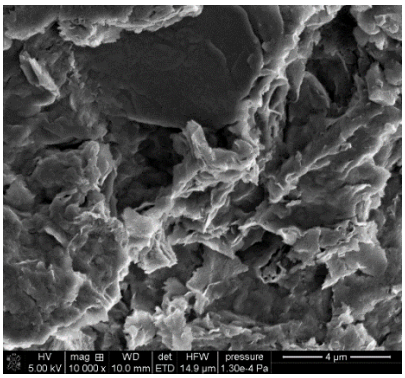
RFR-78

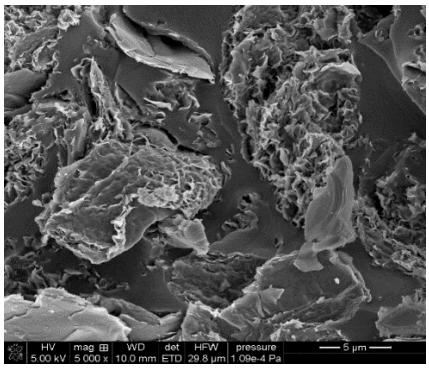
RFC-78

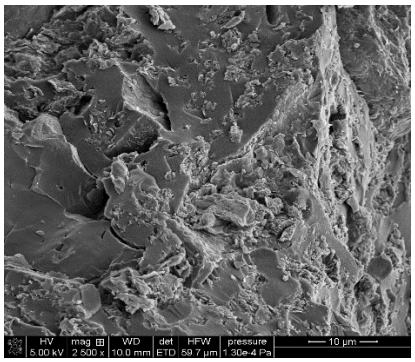
RFR-79

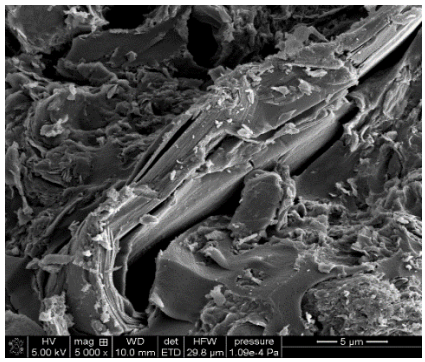
RFC-79

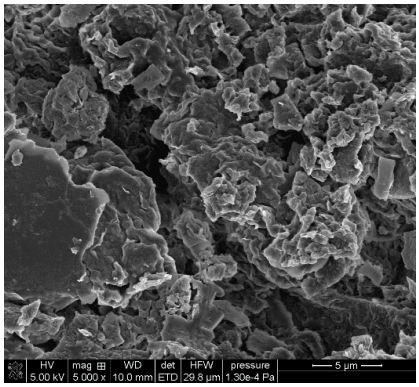
RFR-80

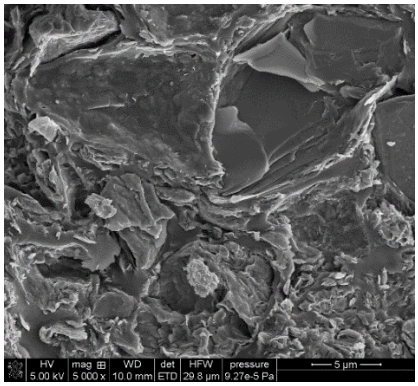
RFC-80

Figure S4. SEM images of nanocomposites.

Fourier Transform Infrared Spectroscopy (FTIR) was used to analyze the gaseous products of sample combustion in order to understand the effects of weight loss and gas evolution during thermal destruction. Gram Schmidt curves illustrate the presence of gases that are released during thermal decomposition processes. As seen from the Figure S4, these curves contain peaks in the range of 200-600 ° C, which represent the amount of gas emitted during

carbon combustion. It is worth noting that the position and change in their intensity coincide with the DTG curves (Figure S5).

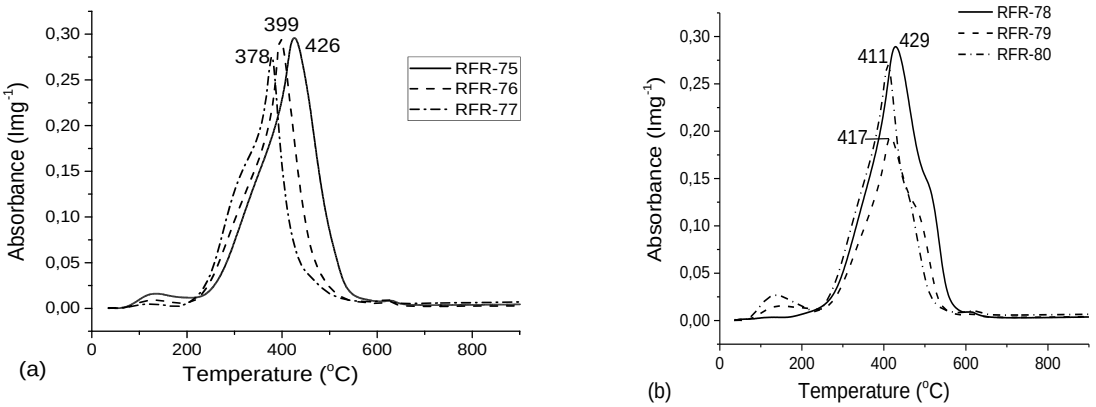

Figure S5. Gram-Schmidt curves for the combustion of samples of first (a) and second (b) series.

References

1. Pujari, P.K.; Sen, D., Amarendra, G.; Abhaya, S.; Pandey, A.K.; Dutta, D. Study of pore structure in grafted polymer membranes using slow positron beam and small-angle X-ray scattering techniques. *Nuclear. Instr. Method Phys. Res. B*. **2007,** 254, 278–282; DOI: 10.1016/j.nimb.2006.11.052;
2. Provencher S.W.; A constrained regularization method for inverting data represented by linear algebraic or integral equations. *Comp. Phys. Comm.* **1982**, 27, 213-227; DOI:10.1016/0010-4655(82)90173-4;
3. Brumberger H. *Small Angle X-ray Scattering*; Brumberger H.: Gordon & Breach, New York, Syracuse, **1965**; p. 509;
4. Dieudonné, Ph.; Hafidi, A.A.; Delord, P.; Phalippou, J. Transformation of nanostructure of silica gels during drying. *J. Non-Crystal. Solid.* **2000**, 262, 155-161; DOI:10.1016/S0022-3093(99)00687-0;
5. Fairén-Jiménez, D.; Carrasco-Marín, F.; Djurado, D.; Bley, F.; Ehrburger-Dolle, F.; Moreno-Castilla, C. Surface area and microporosity of carbon aerogels from gas adsorption and small- and wide-angle X-ray scattering measurements, *J. Phys. Chem. B.* **2006,** 110, 8681-8688; DOI: 10.1021/jp055992f;
6. Sakurai, S. SAXS evaluation of size distribution for nanoparticles *In X-ray Scattering*; Ares, A.E. Ed.; InTech: Croatia, **2017**, Chapter 5. pp. 107-134; DOI: 10.5772/105981;
7. Gun'ko, V.M.; Composite materials: textural characteristics, *Applied Surface Sci.* **2014**, 307, 444–454; DOI:10.1016/j.apsusc.2014.04.055;
8. Gun'ko, V.M.; Meikle, S.T.; Kozynchenko, O.P.; Tennison, S.R.; Ehrburger-Dolle, F.; Morfin, I.; Mikhalovsky, S.V. Comparative characterization of carbon and polymer adsorbents by SAXS and nitrogen adsorption methods, *J. Phys. Chem. C.* **2011,** 115, 10727-10735; **DOI:** 10.1021/jp201835r;
9. Gun'ko, V.M.; Turov, V.V.; Pakhlov, E.M.; Krupska, T.V.; Charmas, B. Effect of water content on the characteristics of hydro-compacted nanosilica. *Appl. Surf. Sci.* **2018**, 459. 171–178 DOI:10.1016/j.apsusc.2018.07.213;

10. Goliszek, M., Podkościelna, B., Fila, K., Riazanova, A. V., Aminzadeh, S., Sevastyanova, O., Gun'ko, V.M. Synthesis and structure characterization of polymeric nanoporous microspheres with lignin. *Cellulose.* **2018**, 25(10), 5843–5862; DOI: 10.1007/s10570-018-2009-7;
11. Gun'ko, V.M., Turov, V.V.; Pakhlov, E.M.; Krupska, T.V.; Borysenko, M.V.; Kartel, M.T.; Charmas, B. Water interactions with hydrophobic versus hydrophilic nanosilica. *Langmuir*. **2018**, 34, 12145–12153; DOI: 10.1021/acs.langmuir.8b03110.